Orographical Effects of Heavy Rainfall by Typhoon 0514 (NABI)

Kenji Tanaka[1], Sayaka Kamohara[2], Fumihiko Yamada[3], Terunori Ohmoto[4] and Satoru Sugio[5]

Abstract: Numerical experiments using a mesoscale meteorological model (MM5) are performed to evaluate the mountainous orographical effects on the heavy rainfalls brought by Typhoon 0514 (NABI), which caused the flood disaster in the southeast Kyushu area of Japan. The terrain conditions considered in the numerical model are three folds: first, a flat terrain with the altitude 1m above mean sea level; second, an idealized line-shaped mountain terrain; third, a complex terrain using GTOPO30. Although an accumulated rainfall due to Typhoon 0514 is recorded higher than 1,000 mm, a calculated one using the flat terrain is 250-300 mm. The calculated rainfall using the complex terrain becomes 200-300% (500-900 mm) in comparison to flat terrain case. This discrepancy is found to cause by blocking and evolving the convective cells, which are generated by lifting up the water vapor along the mountain slope in the windward areas. A ratio of the forecasted rainfall with/without orography provided an important index for the risk of the heavy rain in the tropical cyclone.

Keywords: Heavy rainfall, lifted condensation, mesoscale meteorological model (MM5), orographical rainfall, Typhoon 0514 (NABI)

---

[1] Assistant Professor, Department of Civil and Environmental Engineering, Graduate School of Science and Technology, Kumamoto University, Kurokami 2-39-1, Kumamoto city, Kumamoto, 860-0862, Japan (corresponding author). E-mail: ktanaka@gpo.kumamoto-u.ac.jp

[2] Graduate Student, Department of Civil and Environmental Engineering, Graduate School of Science and Technology, Kumamoto University, Kurokami 2-39-1, Kumamoto city, Kumamoto, 860-0862, Japan.

[3] Associate Professor, Department of Civil and Environmental Engineering, Graduate School of Science and Technology, Kumamoto University, Kurokami 2-39-1, Kumamoto city, Kumamoto, 860-0862, Japan. E-mail: yamada@gpo.kumamoto-u.ac.jp

[4] Professor, Department of Civil and Environmental Engineering, Graduate School of Science and Technology, Kumamoto University, Kurokami 2-39-1, Kumamoto city, Kumamoto, 860-0862, Japan. E-mail: ohmoto@gpo.kumamoto-u.ac.jp

[5] Department of Civil Engineering, Faculty of Engineering, Miyazaki University, Gakuen-Kihanadai-Nishi 1-1, Miyazaki city, Miyazaki, 889-2192, Japan. E-mail: sugio@civil.miyazaki-u.ac.jp

Introduction

Typhoon 0514 (T0514, NABI) occurred to the far southeast of Japan on 29 August 2005. T0514 was evolved while moving westward around the 20º N zone; turn to the north on 3 September; and landed on the west of Kyushu Island on 6 September. The typhoon and the stationary front located just north of the typhoon brought heavy rainfall over the coastal region of the Pacific Ocean in Japan in early September, 2005. In the east Kyushu, the accumulated rainfall was recorded higher than 1,000 mm, and recorded the highest 24-hr or 72-hr rainfall at much of the ground observation stations. By T0514 and the stationary front, 29 lives were lost and 23,572 residences were flooded in the whole of Japan. Much of the damage was concentrated in the east of Kyushu, the number of which is listed in Table 1.

According to Urgent Research Party of T0514 disaster JSCE (2006), three major factors can be thought to bringing such a record rainfall: a) the interaction between the Typhoon and the front (the satellite image shown in Fig. 1), b) the long duration staying inside of the typhoon rainband system, and c) the local effect such as the orographical effect. The interaction between the typhoon and the stationary front has often brought heavy rain in the southeast areas to the front. (e.g. T0420) The warm moist air parcel is supplied to the south east area of the front by the south wind along with the typhoon's circulation. The duration staying inside of the rainband is determined by the horizontal scale and the moving speed of the system itself. The horizontal scale of the T0514 was rather large: the radius of the wind speed higher than 15 m/s was larger than 700 km. The moving speed of the typhoon system itself was about 15—20 km/h (4—6 m/s). Such slow speed and large horizontal scale makes the duration inside the rainband more than 36 hours over west Japan. As shown in Fig. 2, Kyushu Islands has a mountain range running from northeast to south of the island. The mean altitude of the mountain top is about 1,200 m, which was higher than the lifting condensation level inside the typhoon system.

The structure of the precipitation system inside the typhoon was discussed by many authors (e.g., Kurihara and Tuera, 1974; Lin et al., 1999; Liu et al., 1997, 1999; Yamasaki 2005). A number of the orographic rainfall mechanisms has been documented (e.g., Mass, 1981; Grossman and Durran, 1984; Pandey et al., 2000; Colle, 2004). However, there has been little on the orographic rainfall inside the typhoon system. To develop the method for evaluating the orographical component of the typhoon rainfall system will bring the information on local scale potential of the flood and boulder flow. Mesoscale meteorological models such as MM5 and ARPS are useful tools for the numerical evaluation. These numerical models compute the atmospheric fields using the land-surface information such as terrain, soil physical properties, and vegetation.

This study is aimed to evaluate the mountainous orographical effects on the heavy rainfall brought by the Typhoon NABI (T0514), which hit the Kyushu Island Japan on 6 September 2005. Three kinds of terrain conditions are given in the numerical experiment using mesoscale meteorological model: first, a flat terrain with the altitude 1m above mean sea level; second, an idealized line-shaped mountain terrain; and third, a complex terrain using GTOPO30. A ratio of the rainfall under the complex terrain under the flat terrain is computed to evaluate the stationary risk of heavy rainfall. Overview of observation record will be described first. Then, the overview of numerical model and experimental design of the present study will be described. Next, the computed result will be shown and the mechanism of the orographical precipitation system will be discussed. After discussion, the present study will be concluded.

Overview of observation records

The report on the disaster itself was provided by Ushiyama and Fujiyoshi (2005) in Japanese, with the use of the JMA ground observation data archives named as AMeDAS.

Here gives the overview of meteorological record briefly.

The time altitude cross section of the horizontal wind is shown in Fig. 3, observed at Kumamoto meteorological station. Wind from east or southeast began to blow at 00 UTC Sep. 5, implying of coming inside the typhoon cyclonic system. As the typhoon came close during the local daytime on Sep. 6, the wind direction turned to south or southwest. The wind vector on Sep. 4 represented the base state of the upper air wind surrounding of the typhoon over south Japan. The high pressure system covered over Pacific Ocean and East China Sea on Sep 4 and the upper air wind was as weak as 10 m/s.

Fig. 4 shows the accumulated rainfall of Radar-AMeDAS grid point value (GPV) during 72 hours from 0900 UTC 3 Sep. to 0900 UTC 6 Sep. 2005 (i.e., from 0000 JST 4 Sep. to 0000 JST 7 Sep. 2005). The Radar-AMeDAS GPV data is the grid point value generated from the Doppler radar observation and the JMA AMeDAS rainfall observation with the horizontal resolution about 2.5 km. Both of the data shows the clear contrast between the east and west side of the mountain range. The 72-hour rainfall was higher than 500 mm over the east Kyushu region. In several mountain areas of the east Kyushu, the rainfall exceeded to 1,000 mm. In the west of Kyushu, on the other hand, the 72-hour rainfall was lower than 200 mm.

Mikado area in the Middle East Kyushu (see Fig. 2) was the one of the record rainfall area. According to the observation network of the JMA (AMeDAS), the 72-hr rainfall was as high as 1,320 mm, which is about as half as the annual rainfall in the same area. Fig. 5 shows the variation of the ground rainfall of the JMA-AMeDAS Mikado station (32º23.1′ N 131º19.9′E alt. 250 m). The hourly rainfall increased linearly since 1800 UTC on Sep 4, and the hourly rainfall became maxima at 0000 UTC on Sep 6. Most of the rainfall was brought till 0300 UTC on Sep. 6 when the center came close most to the area.

Mesoscale Model

The Fifth Generation Penn-State/NCAR Mesoscale Model (MM5) (Grell et al. 1994; Dudhia et al., 2005) is one of the non-hydrostatic meteorological models. MM5 is now used for not only the scientific study on the evolution of precipitation system, but the application to the ocean wave prediction. MM5 contains a capability of multiple nesting with two-way interaction. Such nesting technology can compute both the large scale disturbance with horizontal scale larger than 1,000 km in coarse domain and the small scale disturbances with the scale of several kilometers in nested domain at once.

The MM5 used so called as terrain-followed σ-coordinate system in the vertical direction defined by pressure (p) as

$$\sigma = \frac{p_0 - p_t}{p_{s0} - p_t} \qquad (1),$$

where p_0 = pressure at reference-state level (e.g. 1,000 hPa, 500 hPa); p_t = pressure at top level; and p_{s0} = at surface reference-state surface pressure, respectively. The basic equations of MM5 are as follows:

$$\frac{\partial p'}{\partial t} - \rho_0 g w + \gamma p \nabla \cdot \mathbf{v} = -\mathbf{v} \cdot \nabla p' + \frac{\gamma p'}{T}\left(\frac{\dot{Q}}{c_p} + \frac{T_0}{\theta_0} D_\theta \right) \qquad (2)$$

$$\frac{\partial u}{\partial t} + \frac{m}{\rho}\left(\frac{\partial p'}{\partial x} - \frac{\sigma}{p^*}\frac{\partial p^*}{\partial x}\frac{\partial p'}{\partial \sigma} \right) = -\mathbf{v} \cdot \nabla u + v\left(f + u\frac{\partial m}{\partial y} - v\frac{\partial m}{\partial x} \right) - ew\cos\alpha - \frac{uw}{r_{earth}} + D_u \qquad (3)$$

$$\frac{\partial v}{\partial t} + \frac{m}{\rho}\left(\frac{\partial p'}{\partial y} - \frac{\sigma}{p^*}\frac{\partial p^*}{\partial y}\frac{\partial p'}{\partial \sigma} \right) = -\mathbf{v} \cdot \nabla v - u\left(f + u\frac{\partial m}{\partial y} - v\frac{\partial m}{\partial x} \right) + ew\sin\alpha - \frac{vw}{r_{earth}} + D_v \qquad (4)$$

$$\frac{\partial w}{\partial t} - \frac{\rho_0}{\rho}\frac{g}{p^*}\frac{\partial p'}{\partial \sigma} + \frac{g p'}{\gamma p} = -\mathbf{v} \cdot \nabla w + g\frac{p_0}{p}\frac{T'}{T_0} - \frac{g R_d}{c_p}\frac{p'}{p} - e\left(u\cos\alpha - v\sin\alpha \right) + \frac{u^2 + v^2}{r_{earth}} + D_u \qquad (5)$$

$$\frac{\partial T}{\partial t} = -\mathbf{v} \cdot \nabla T + \frac{1}{\rho c_p}\left(\frac{\partial p}{\partial t} + \mathbf{v} \cdot \nabla p' - \rho_0 g w \right) + \frac{Q}{c_p} + \frac{T_0}{\theta_0} D_\theta \qquad (6)$$

Eqs. (2)-(6) represent the equation of pressure, momentum of *x,y,z*-component, and thermodynamics, respectively. Symbols in these equations are represented as following: **v** = wind vector with the component of (*u,v,w*); *g* = acceleration of the gravity; *f* (= 2Ωsinϕ) and *e* (= 2Ωcosλ) are Coriolis parameters at latitude ϕ and at longitude λ; α = the latitude difference; c_p = the heat capacity of dry air under constant pressure; ρ = the atmospheric density; R_d is the gas constant for dry air; $\gamma = R_d/c_p$, ; *m* = map projection factor; *p'* = pressure perturbation at reference pressure level, p_0; *p** = pressure difference between top and ground surface (p_{s0}-p_t) ; *Q* = heat energy into the air parcel; $\dot{Q}$ = time rate of *Q*; and D = diffusion term for each variable *u, v, w,* and θ, respectively.

The equation of the moisture can be written as

$$\frac{\partial q_a}{\partial t} = -m^2\left[\frac{\partial p^* u q_a/m}{\partial x} + \frac{\partial p^* v q_a/m}{\partial y}\right] - \frac{\partial p^* q_a \dot{\sigma}}{\partial \sigma} + \delta_{nh}\left[m^2\left[\frac{\partial p^* u/m}{\partial x} + \frac{\partial p^* v/m}{\partial y}\right] + \frac{\partial p^* \dot{\sigma}}{\partial \sigma}\right] + p^* \Delta q + D_{qp} \quad (7)$$

, where q_p= the mixing ratio for each phase *a* (water vapor, cloud liquid water, rain water etc.); δ_{nh}= the nonhydrostatic run switch (=1: nonhydrostatic run, or =0: hydrostatic run); Δ*q*= the rate of the phase change; $\dot{\sigma}$ = time rate of σ, respectively. Eight kinds of moisture physics option are available in the MM5 according to the moisture phase change process (Dudhia, 1989; Reisner et al., 1988; Tao and Simpson, 1993; Schultz, 1995). Eight kinds of option are available on cumulus parameterization accordingly with horizontal grid size (Betts and Miller, 1993; Fritsch and Chappell, 1980; Grell et al. 1994; Kain and Fritcsh, 1993; Kain 2002).

For the surface boundary condition, MRF PBL-model (e.g., Hong and Pan, 1996; Chen and Dudhia, 2001) was used to compute the planetary boundary layer (PBL) processes and five-layer land surface model was used (Dudhia, 1989) to compute surface soil layer process.

To generate the lateral boundary for the coarse domain and the initial condition, the grid point value (GPV) data such as NCEP Reanalysis are required.

Experimental design

Two-level domain is defined in the present study shown in Fig. 6. The line A—A' is defined for the analysis of the atmospheric vertical structure as discussed later. The horizontal grid interval for each domain is 9 km and 3 km, respectively. The JMA-MANAL with 10-km horizontal resolution was used for the atmospheric GPV. The New Generation Sea Surface Temperature (NGSST) (Sakaida et al., 1998; Tanahashi et al., 2000) was used for the sea surface temperature dataset. The model start time was set as 00 UTC 04 Sep. 2005 and forecasted 72 hours. During first 24 hours, the meteorological fields were forecasted only in DOMAIN 1. After that, DOMAIN 1 and DOMAIN 2 were computed with the two-way interaction. The time step of DOMAIN 1 was 10 seconds, which was divided into three small time steps for computing DOMAIN 2. Simple ice scheme (Dudhia, 1989) is used to compute the atmospheric moisture process. Because of the horizontal grid size (<10 km), no cumulus parameterization was used.

Five runs were performed in this study with various kinds of terrain condition. First, flat terrain condition with the altitude 1m above mean sea level was used to investigate without orographical effect (Run-1). To discuss the orographical effect simply, a line-shaped mountain range was assumed. The crest of the mountain range is designed as the line B—B' in Fig. 6. The altitude was given as a function of the horizontal distance from the crest of the mountain as

$$H(x) = H_{plane} + \frac{\Delta H}{2}\left(1+\cos\left(\frac{x-x_0}{r}\pi\right)\right) \quad \text{for } |x\text{-}x_0| < r \qquad (8),$$

where H_{plane} = the altitude of the land surface outside the mountain range (=1 m); ΔH= the mountain height relative to the plane; r = the half side width of the mountain range (= 45 km); x_0 the location of the crest respectively. The condition with ΔH = 1,200 m (average from the real terrain) (Run-2a), 500 m (Run-2b), and 200 m (Run-2c) were computed to compare the lifting of moisture. The last run (Run-3) is the case of complex terrain, using a global coverage topography data, GTOPO30 provided by the United States Geoloical Survey (USGS).

Results

Fig. 7 shows the computed typhoon tracks of Run-1, Run-2a, and Run-3. JMA best track is also plotted in the same figure. According to this figure, these experiments obtained a very good track position, especially when the eye of the typhoon was moving on the ocean. The computed track is likely to move east after the landfall as compared to the JMA best track. Xiao et al. (2006) made a numerical experiment on Typhoon Rusa (2002) using MM5 and resulted that the deviation between computed track and JMA best track were about 50—100 km in average with the bogus data assimilation. In this study, the deviation between computed tracks and JMA best track was smaller than 100 km and quite reasonable as compared to that of Xiao et al. (2006).

The accumulated rainfall was computed as an integrated value of precipitation rate from the beginning of the computation (00 UTC 4 Sep. 2005) to the end of DOMAIN2 computation (15 UTC 6 Sep. 2005). The accumulated rainfall of Run-1 and that of Run-3 are shown in Fig. 8. Without the orographical effect, the accumulated rainfall was smaller than 350 mm in whole area of the southeast Kyushu Island. The rainfall of the inner Kyushu Island was a little higher than that of surrounding. One of the reasons is the distribution of the land-sea surface cover, which controls the surface roughness length and

bowen ratio (i.e. latent heat flux from surface). With the complex terrain in Run-3, the accumulated rainfall became higher than 800 mm on the east mountainside. Meanwhile, the rainfall which was smaller than 100 mm was extended widely into the west coastal area of Kyushu Island.

To clarify the orographical effect, accumulated rainfall of each run (except Run-1) was normalized by that of Run-1. Fig. 9 shows the distribution of normalized accumulated rainfall. Respectively, labels B and B' on the panel of Run-2a, 2b, and 2c denote the south and north end of the linear-shaped crest. The normalized accumulated rainfall of Radar-AMeDAS GPV is also shown in this figure. It is obvious that the mountain range controlled the rainfall at ground level in Fig. 9. As the top of the crest set higher, the ratio became higher in the east mountainside; on the other hand, the ratio became lower in the west mountain side. In Run-2c with the top of the mountain 200 m, the most of region was covered with the ratio between 60—150%. However, in Run-2b with the top of the mountain 500 m a.s.l., there existed the zone with the ratio higher than 200 % just east of the crest, and existed the zone with the ratio less than 50% in the coastal area of Yatsushiro and Ariake Sea. More significantly, with the top of the mountain 1,200 m a.s.l. in Run-2a, the ratio higher than 250% spread widely in the east mountainside, while the ratio was smaller than 20% in the whole area of Yatsushiro Sea. As mentioned above, the most of the rainfall brought inside the foreside of the typhoon system, provided warm moist air from Pacific Ocean with southeast wind. Hence, this result showed that the moisture blocking by the mountain range played a significant role, with the high anomaly in the windward mountainside and the low anomaly in the leeward area. The mechanism of the blocking process will be discussed later.

The complex terrain condition in Run-3 brought more heterogeneous rainfall ratio. In the east of Kyushu Island, the high anomaly area (higher than 200%) was good

correspondence with the area of altitude higher than 500 m. The anomalies higher than 300% were seen in the northeast area of the domain. Although it was likely to underestimate of the rainfall in the south area of the domain as compared to that of Radar-AMeDAS GPV, the computational result of Run-3 provided rather good evaluation of rainfall in the northeast of the domain.

Fig. 10 shows the snapshots of the past 1-hr rainfall with the center of the typhoon located to the west of South Kyushu. Without the mountain orography (Run-1), the distribution of rainfall showed the general structure of the typhoon system. Arc-shaped rainbands can be seen near the center of the eye and around north end of the domain in this figure. Such arc-shaped rainbands were blocked by the mountain orography as shown clearly in the snapshot of Run-3. The windward slope in the East Kyushu, the rainfall was more intensified. In the meanwhile, no rain area was extended from the north of Yatsushiro Sea to the south of Ariake Sea.

Area averages of the accumulated rainfall over DOMAIN2 of each run and of Radar-AMeDAS are shown in Fig. 11. The area average of rainfall was ranged between 250 mm and 310 mm. The average rainfall with the mountain orography was higher by 20 % than that with flat terrain. This rate of the area average rainfall was about one-tenth of the maximum horizontal distortion (~250%). Therefore, the surface orography produced the effect of the contrast between windward and lee side much greater than an increase effect of space average rainfall.

Computed rainfall for each run is compared with the observed rainfall at Mikado Area in Fig. 12. Without the mountain orography (Run-1), the computed rainfall was as small as one third of the ground observed rainfall, and less than half of the Radar-AMeDAS reanalysis. With the complex terrain (Run-3), the computed rainfall was smaller by about 20—40 % than the ground based observation. However, comparing with the

Radar-AMeDAS rainfall, the computed rainfall of Run-3 is about 10 % higher than the reanalysis value. Considering the horizontal resolution, Run-3 yielded a reasonable estimation as compared to the Radar-AMeDAS rainfall.

Vertical structure of the precipitation system

From above results, it was clear that the mountain orography gave a significant effect in bringing the heavy rain over the windward side. Here will discuss the mechanism of the orographical rainfall system by vertical profile of moisture and wind.

Fig. 13 shows the vertical cross section (line A—A' in Fig. 6) of the cloud water content (CWC) and of the rainwater content for Run-1, Run-2a and Run-3. Darkness shows the CWC, and contour line shows the rainwater with the interval of 0.5g/kg. The rainy atmosphere with the rainwater higher than 1.0 g/kg is hatched. It should be noticed that the west end of the DOMAIN2 is taken as origin in the horizontal axis. The wind vector with eastward and vertical component is shown in the same figures. The surface elevation is shown in the bottom of the panel. There are cloudless layers between 300 hPa and 500 hPa isobaric surfaces, where the lifted moisture changes into rainwater and begins to drop. The vertical distribution of the cloud liquid water and rainwater of Run-1 showed that there was little local scale convection without the mountain orography. Although the evolved cumulus system was seen above Amakusa Islands (Y = 70 km) and Yatsushiro Sea (Y = 120 km), the rainwater of the lower atmosphere was smaller than 0.5 g/kg over that area. In Run-2-a, a convection cell with the CLWC higher than 0.5 g/kg can be seen in the windward side of the mountain (Y = 170—210 km), i.e. around Mikado Area. In that windward area, updraft along the mountain slope was evolved between the ground surface and 500 hPa plane. The lifted moisture was forced to make condensation rapidly and to drop as a rain. Such convective system evolved stationary as the typhoon cloud system moved to north.

The dry air after dropped rainwater ran through the west slope and reached to Yatsushiro Sea. Another convective cloud system was evolved above the coastal area of Yatsushiro Sea (Y = 90—120 km). This cloud system was evolved by a updraft generated from a mountain wave. But the rainwater was brown westward by the typhoon east wind. Assuming that the raindrop terminal velocity is 7 m/s (typical value with the raindrop diameter of 1 mm), the raindrop from 7 km a.s.l. brown westward 30 km away, was under the easterly wind of 30 m/s. Similar convective cell can be seen in the result of Run-3. Hence, the mountain orography is important in the evolution of the local stationary convective cloud system inside the typhoon system by lifting up the lower moist air parcel mandatory.

Atmospheric moisture fields are also important in the evolution of convective cell. Table 2 summarizes the physical indices observed by Rawinsonde at Kagoshima station. The difference between the pressure at mean sea level (PMSL) and the lifted condensation level (LCL) was 65—75 hPa, equivalent to 700—800 m in height. Hence, the LCL was lower than the crest of the Kyushu Mountain range (1,200—1,700 m). The level of free convection (LFC) was ranged about 1,500—2,500 m inside the typhoon cloud system. The LFC was as the same as or little higher than the crest of the Kyushu Mountain range. According to the convective available potential energy (CAPE) and the convective inhabitation (CIN), there was not so much unstable inside the typhoon rainband system. If the air near at ground level was dry, LCL and LFC became much higher, and effect of the orographical lifting was much weaker. Hence the moisture at low level atmosphere is quite important in determining whether the mountain height reached LCL or LFC and affected the convective cell with a heavy rain.

Conclusion

The present study evaluated the orographical effect of the heavy rainfall brought by

the typhoon NABI (T0514), using the numerical model. The mountain orography played an important role in bringing a heavy rainfall over the East Kyushu Area, by blocking and convecting warm moist air supplied from Pacific Ocean. The numerical experiment with the flat terrain condition found out that the meteorological system of the typhoon and the front itself brought 250—300 mm in total rainfall. With the mountain orography, the precipitation water was arranged intensively in the windward mountainside (~300% in anomaly) and sparsely (~50% in anomaly) in the leeward low-level area. The area averaged rainfall including both the windward mountainside and the leeward area did not depend significantly on the terrain condition. That is, the effect of the heterogeneous distribution was much more significant. The local stationary convective cells evolved over the windward (east) side of the mountain slope. These cells brought a heavy rain with the rate higher than 20 mm/hr continuously and brought a flood disaster.

Complex surface condition made the distribution of the rainfall more complex. In the present study, the horizontal grid interval was set as 3 km, which are usual in the computation of the terrain effect. The present computation with the complex topography data resulted in good evaluation of accumulated rainfall for the considerable extent. In order to make more accurate evaluation as compared to the observed rainfall distribution, it is required to improve the horizontal (and vertical) grid spacing, to use the more accurate SST with the diurnal scale variation (may not be practical in the current state), to use the more accurate land use database, and to study the bulk microphysical parameterization, and so on. However, the result of the present study provides the technique of evaluating the local scale risk distribution of the heavy rainfall in coming close the tropical cyclone: a ratio between the computed rainfall with and without terrain data. As the ratio is evaluated higher, the risk of heavy rain becomes higher. Such index will be helpful for deciding the priority region especially including mountains.

Acknowledgement

The authors would like to acknowledge to Miyazaki, Kagoshima and Kumamoto Prefecture Office for providing the meteorological observation data. This study was supported from a grant of the Foundation of the River and Watershed Environment Management and the grant of Kumamoto Society of Natural Disaster.

References

Betts, A. K., and Miller, M. J. (1993). "The Betts-Miller scheme. The representation of cumulus convection in numerical models", K. A. Emanuel and D. J. Raymond, Eds., *Amer. Meteor. Soc.*, 246 pp.

Chen, F., and Dudhia, J. (2001). "Coupling an advanced land-surface/hydrology model with the Penn State/NCAR MM5 modeling system Part I: Model implementation and sensitivity." *Mon. Wea. Rev.*, 129, 560-585.

Colle, B.A. (2004). "Sensitivity of orographic precipitation to changing ambient conditions and terrain geometries: an idealized modeling perspective," *J. Atmos. Sci.*, **61**, 588-606.

Dudhia, J. (1989). "Numerical study of convection observed during the winter monsoon experiment using a mesoscale two-dimensional model." *J. Atmos. Sci.*, **46**, 3077-3107.

Dudhia, J., Gill, D., Manning, K., Wang, W., Bruyere, C., Kelly S., and Lackey, K., (2005). *PSU/NCAR Mesoscale Modeling System Tutorial Class Notes and User's Guide—MM5 Modeling System Version 3*, National Center for Atmospheric Research <www.mmm.ucar.edu/mm5>.

Grell, G.A., Dudhia J., and Stauffer D.R, (1994). *A description of the fifth-generation Penn State NCAR mesoscale model (MM5)*. NCAR Technical Note, NCAR/TN-398+STR, 117p.

Grossman, P.A. and Durran, D.R. (1984). "Interaction of low-level flow with the Western Ghat Mountains and offshore convection in the summer monsoon." *Mon. Wea. Rev.*, **112**, 652-672.

Hong S-Y., and Pan H-L (1996). "Nonlocal boundary layer vertical diffusion in a medium-range forecast model." *Mon. Wea. Rev.*, **124**, 2322-23339.

Kain, J. S., and J. M. Fritsch, (1993). "Convective parameterization for mesoscale models: The Kain-Fritsch scheme. The representation of cumulus convection in numerical models", K. A. Emanuel and D. J. Raymond, Eds., *Amer. Meteor. Soc.*, 246 pp.

Kain, J. S., (2002). "The Kain-Fritsch convective parameterization: An update." *J. Appl. Meteor.*, **43**, 170-181.

Kurihara Y., and Tuera, R.E. (1974). "Structure of a tropical cyclone developed in a three-dimensional numerical simulation model." *J. Meteor. Soc. Japan,* **31**, 893-919.

Lin, Y-L., Han, J., and Hamilton, D.W. (1999). "Orographic influence on a drifting cyclone." *J. Atmos. Sci.*, **56**, 534-561.

Liu Y., Zhang, D-L., and Yau, M.K.(1997). "A multi scale numerical study of Hurricane Andrew (1992). Part I: Explicit simulation and verification." *Mon. Wea. Rev*., **125**, 3073-3093.

Liu Y., Zhang, D-L., and Yau, M.K. (1999). "A multiscale numerical study of Hurricane Andrew (1992). Part II: Kinematics and inner-scale structures." *Mon. Wea. Rev.*, **127**, 2597-2916.

Mass, C.E., (1981). "Topographically forced convergence in western Washington State." *Mon. Wea. Rev.*, **130**, 1468-1492.

Pandey, G.R, Cayan, D.R., and Georgakakos, K.P. (1999). "Precipitation structure in the Sierra Nevada of California during winter." *J. Geophys. Res.*, **104**, 12019- 12030.

Reisner, J., Rasmussen, R.J., and Buintjes, R.T., (1998). "Explicit forecasting of supercooled liquid water in winter storms using the MM5 mesoscale model." *Quart. J. Roy. Meteor. Soc.*, **124B**, 1071-1107.

Sakaida, F., Moriyama, M., Murakami, H., Oaku, H., Mitomi, Y., Mukaida, A., and Kawamura, H. (1998). "The sea surface temperature product algorithm of the ocean color and temperature scanner (OCTS) and its accuracy." *J. Ocean.*, **54**, pp. 437-442.

Schultz, P. (1995). “An explicit cloud physics parameterization for operational numerical weather prediction.” *Mon. Wea. Rev.*, **123**, 3331-3343.

Tanahashi, S., Kawamura, H., Matsuura, T., Takahashi, T., and Yusa, H. (2000). “Improved estimates of wide-ranging sea surface temperature from GMS S-VISSR data.” *J. Ocean.*, **56**, pp.345-358.

Tao, W.-K., and Simpson, J. (1993). “Goddard cumulus ensemble model. Part I: model description.” *Terrestrial, Atmospheric and Oceanic Sciences*, **4**, 53-72.

Ushiyama M., and Fujiyoshi, Y., (2005). “Characteristics of a heavy rainfall disaster caused by typhoon No. 0514 and stationary front in September 2005.” *J. Japan Soc. Natural Disaster Sci.*, **24-4**, 487-497. (in Japanese)

Urgent Research Party of T0514 disaster JSCE (2006). *Research Report on the damage investigation of T0514 record rainfall and damage reduction study*. Miyazaki, Japan.

Xiao Q., Kuo, Y-H, Zhang, Y., Barker, D.M., and Won, D.J. (2006). “A tropical cyclone bogus data assimilation scheme in the MM5 3D-Var system and numerical experiments with Typhoon Rusa (2002) near landfall.” *J. Meteor. Soc. Japan*, **84**, 671-689.

Yamasaki, M., (2005). “A study of the mesoscale structure of Typhoon Flo (T9019): a case of COMPARE model intercomparison.” *J. Meteor. Soc. Japan*, **83**, 1057-1084.

Figure and Table captions

Fig. 1: The typhoon system and the stationary front observed by the geostationary meteorological satellite (METEOSAT)

Fig. 2: Elevation map of the Kyushu Island. Typhoon track is shown by bold line with time stamp. Locations of key meteorological stations are also plotted. Alphabetical marks are, (a) Ariake Sea, (b) Amakusa Islands, and (c) Yatsushiro Sea, respectively.

Fig. 3: Time altitude cross section of the horizontal wind at Kumamoto observed by the wind profiler, JMA.

Fig. 4: The accumulated rainfall from 09 UTC 4 Sep. to 09 UTC 7 Sep. 2005 over the south Kyushu Island, Japan (Radar-AMeDAS grid point value).

Fig. 5: Time series of the rainfall on the ground level on the Mikado Area in Miyazaki Prefecture.

Fig. 6: Computation domain in this study. Line A—A' shows the analysis line of the atmospheric vertical structure. Line B—B' shows the crest line of the linear-shaped mountain range in Run-2.

Fig. 7: Computed typhoon tracks of NABI (Run-1, 2a and 3). Typhoon track analyzed by JMA (JMA-BT) is also plotted.

Fig. 8: Accumulated rainfall from the beginning of the computation (00 UTC 4 Sep. 2005) to the end of DOMAIN2 computation (15 UTC 6 Sep. 2005). Only the results of Run-1 (left) and Run-3 (right) are shown.

Fig. 9: Accumulated rainfall for each run and Radar-AMeDAS GPV normalized by that of Run-1. Labels B and B' on the panel of Run-2a, 2b, and 2c denote the south and north end of the linear-shaped crest, respectively.

Fig. 10: Spatial average of accumulated rainfall for whole area of DOMAIN2.

Fig. 11: Time series of the accumulated rainfall from at Mikado Area: comparison between

observed data (Fig. 5) and numerical computation.

Fig. 12: Distribution of rainfall past 1 hour at 00 UTC 6 Sep. 2005.

Fig. 13: Isobar-latitude cross section of the cloud liquid water content (darkness) and rainwater (contour line with interval of 0.5g/kg) content for each run. The rainwater higher than 1.0 g/kg is hatched. Vertical and longitude component of wind are plotted as vector. The altitude of the ground surface is added for each panel. Snapshots at 00UTC 06 Sep. 2005.

Table 1: List of damage caused by T0514 (NABI)

Table 2: The physical indices observed at Kagoshima by rawinsonde. Indices are barometric pressure at mean sea level (PMSL), lifted condensation level (LCL), level of free convection (LFC), convective available potential energy (CAPE), and convective inhabitation (CIN).

Table 1

Category	Whole of Japan	East Kyushu
Personal		
Lost and missing	29	21
Injured seriously	45	13
Injured fair	134	40
Dwelling house		
Full destroyed	1,178	1,163
Half destroyed	3,504	3,349
Partially destroyed	2,770	2,421
Flooded	21,160	7,553

Table 2

Indices	9/5 00Z	9/5 12Z	9/5 18Z
PMSL (hPa)	995.3	984.2	974.0
LCL(hPa)	920.5	910.9	908.5
LFC(hPa)	739.1	839.3	731.2
CAPE(m^2s^{-2})	70.7	111.2	35.4
CIN (m^2s^{-2})	-23.7	-6.6	-12.4

Fig. 1

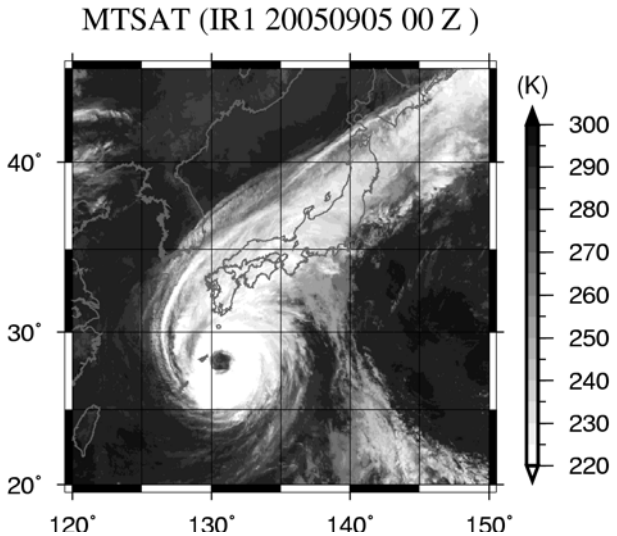
MTSAT (IR1 20050905 00 Z)
(K)
300
290
280
270
260
250
240
230
220
40˚
30˚
20˚
120˚
130˚
140˚
150˚

Fig. 2

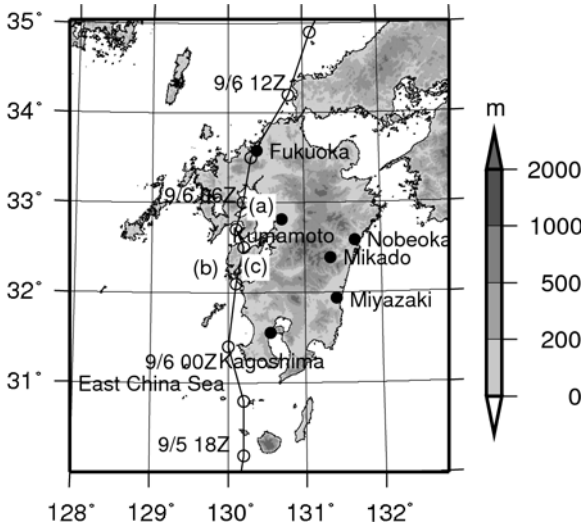
35°
34°
33°
32°
31°
128°
129°
130°
131°
132°
9/6 12Z
Fukuoka
9/6 06Z
(a)
Kumamoto
Nobeoka
Mikado
(b)
(c)
Miyazaki
9/6 00Z
Kagoshima
East China Sea
9/5 18Z
m
2000
1000
500
200
0

Fig. 3

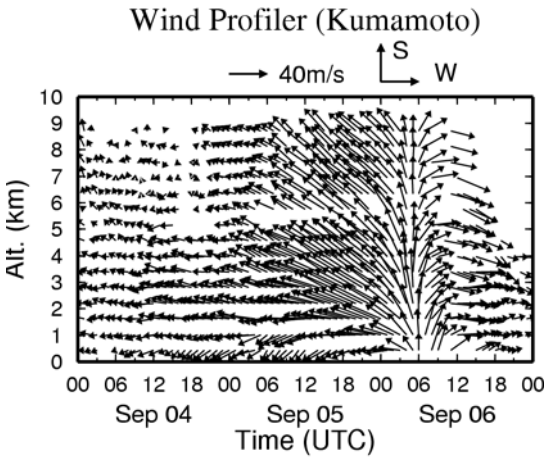
Wind Profiler (Kumamoto)
40m/s
S
W
Alt. (km)
0
1
2
3
4
5
6
7
8
9
10
00 06 12 18 00 06 12 18 00 06 12 18 00
Sep 04
Sep 05
Sep 06
Time (UTC)

Fig. 4

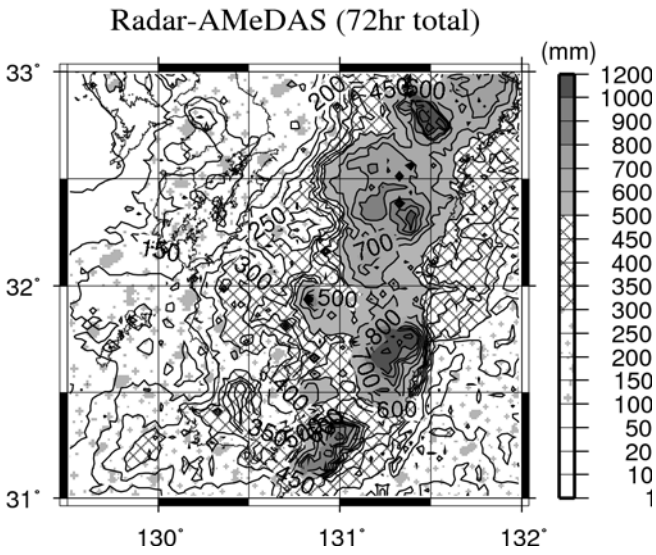
Radar-AMeDAS (72hr total)
(mm)
1200
1000
900
800
700
600
500
450
400
350
300
250
200
150
100
50
20
10
1
33°
32°
31°
130°
131°
132°

Fig. 5

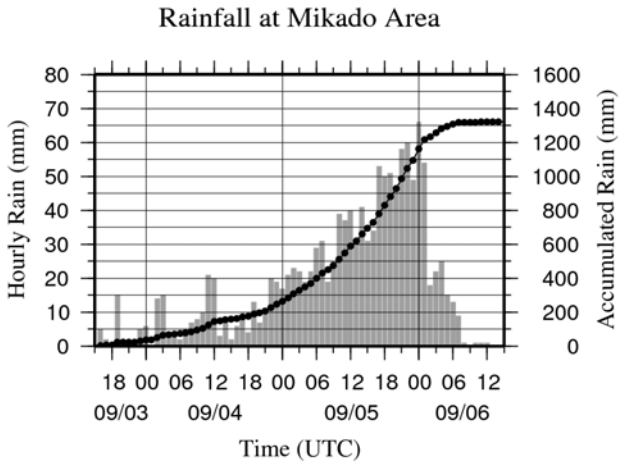
Rainfall at Mikado Area
Hourly Rain (mm)
Accumulated Rain (mm)
0
10
20
30
40
50
60
70
80
0
200
400
600
800
1000
1200
1400
1600
18 00 06 12 18 00 06 12 18 00 06 12
09/03
09/04
09/05
09/06
Time (UTC)

Fig. 6

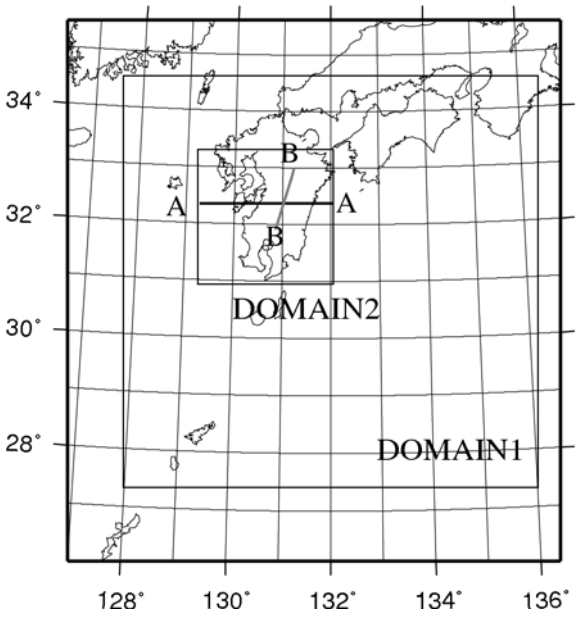

Fig. 7

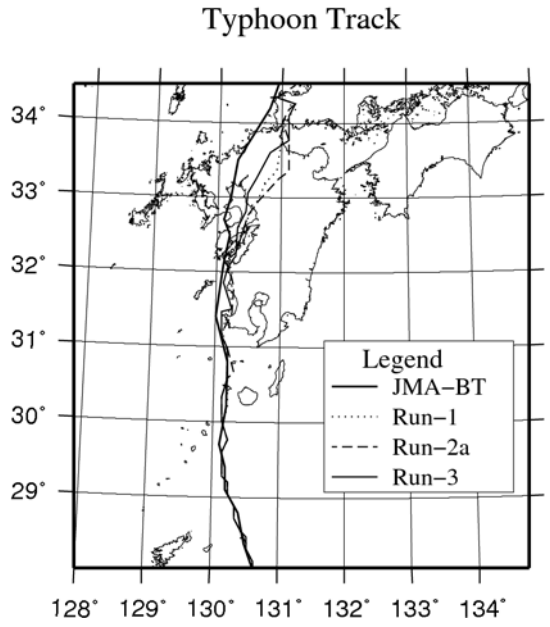
Typhoon Track
34°
33°
32°
31°
30°
29°
128°
129°
130°
131°
132°
133°
134°
Legend
JMA−BT
Run−1
Run−2a
Run−3

Fig. 8

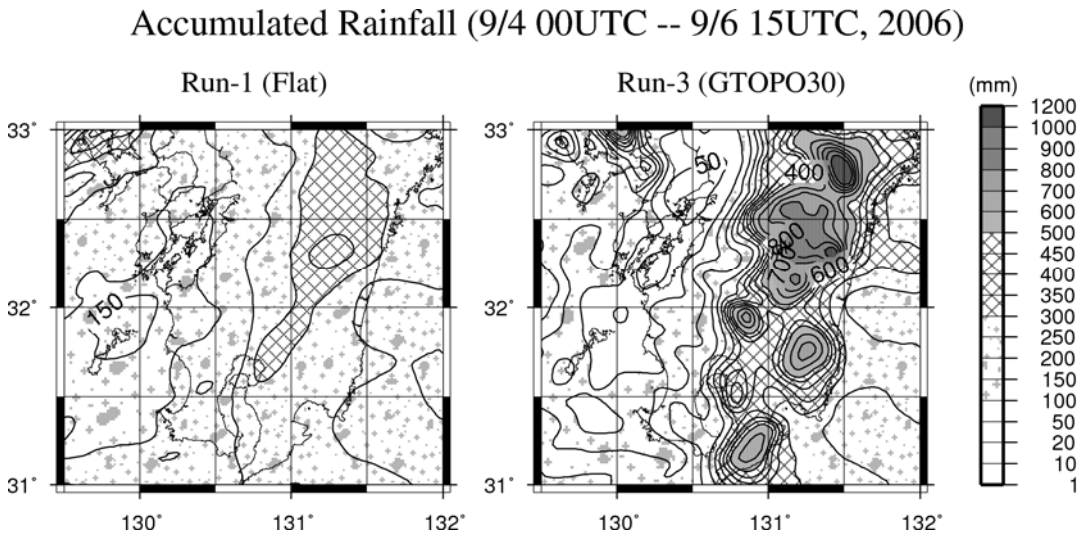
Accumulated Rainfall (9/4 00UTC -- 9/6 15UTC, 2006)
Run-1 (Flat)
Run-3 (GTOPO30)
(mm)
1200
1000
900
800
700
600
500
450
400
350
300
250
200
150
100
50
20
10
1
33°
32°
31°
130°
131°
132°
150
50
400
800
700
600

Fig. 9

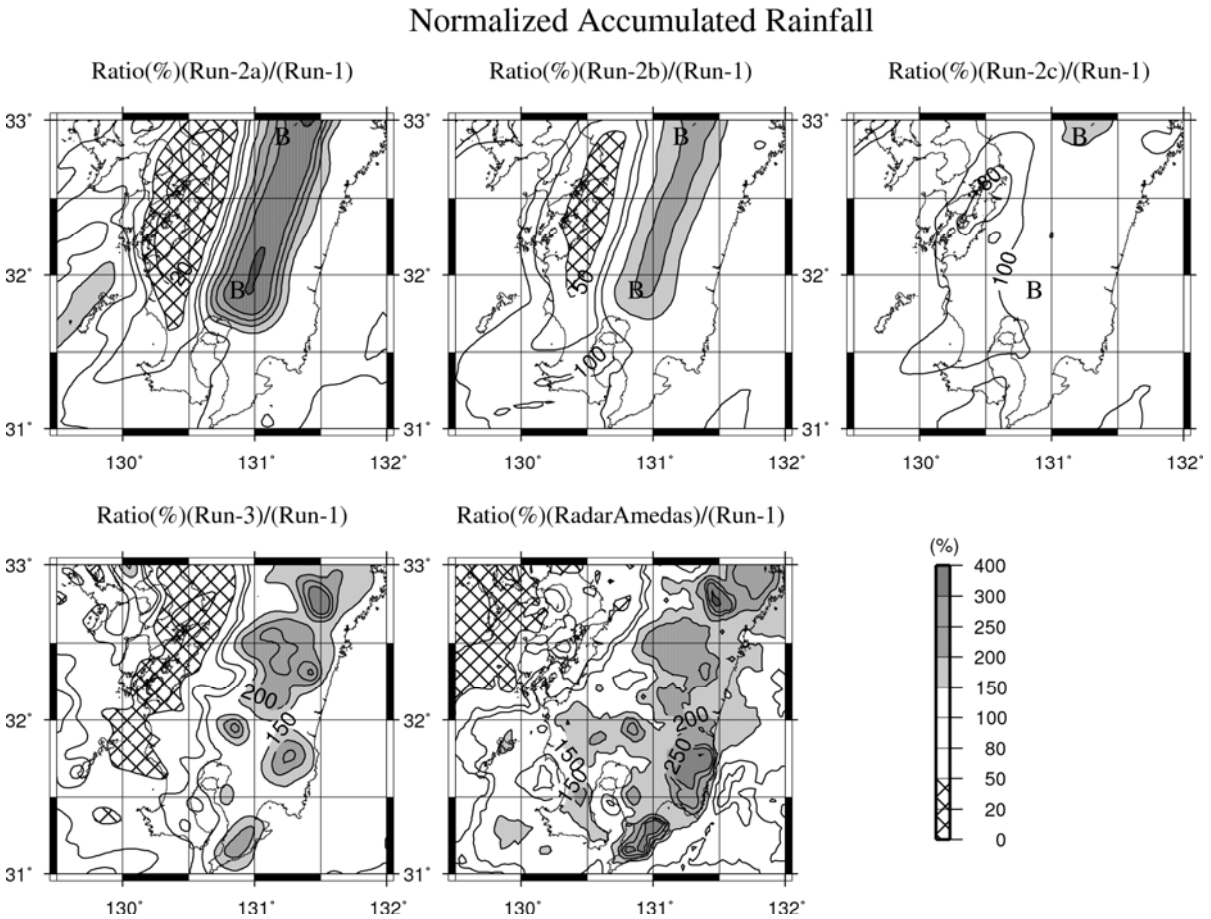
Normalized Accumulated Rainfall
Ratio(%)(Run-2a)/(Run-1)
Ratio(%)(Run-2b)/(Run-1)
Ratio(%)(Run-2c)/(Run-1)
Ratio(%)(Run-3)/(Run-1)
Ratio(%)(RadarAmedas)/(Run-1)
33°
32°
31°
130°
131°
132°
B
50
100
150
200
250
80
(%)
400
300
250
200
150
100
80
50
20
0

Fig. 10

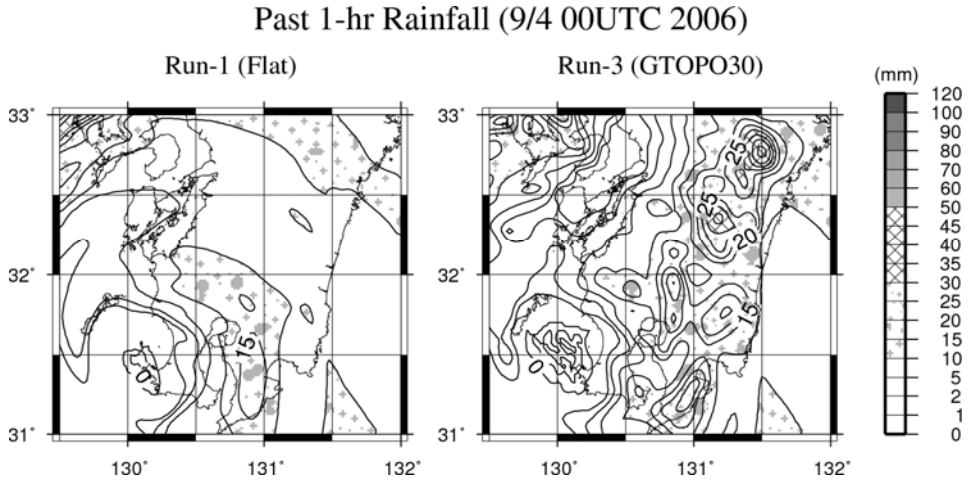
Past 1-hr Rainfall (9/4 00UTC 2006)
Run-1 (Flat)
Run-3 (GTOPO30)
(mm)
120
100
90
80
70
60
50
45
40
35
30
25
20
15
10
5
2
1
0
33°
32°
31°
130°
131°
132°
0
15
25
20

Fig. 11

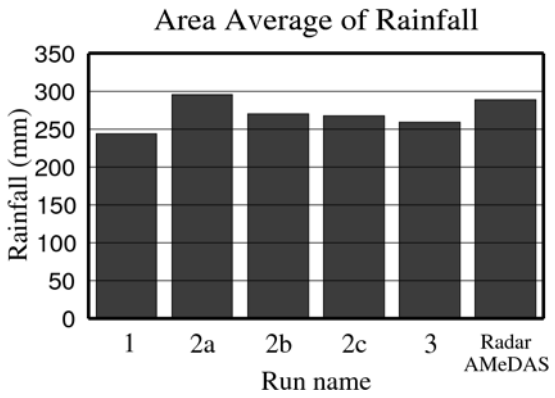
Area Average of Rainfall
Rainfall (mm)
350
300
250
200
150
100
50
0
1
2a
2b
2c
3
Radar AMeDAS
Run name

Fig. 12

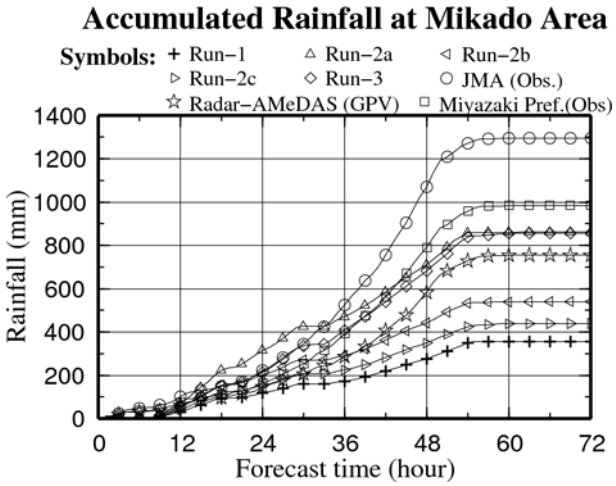
Accumulated Rainfall at Mikado Area
Symbols: Run−1 Run−2a Run−2b
Run−2c Run−3 JMA (Obs.)
Radar−AMeDAS (GPV) Miyazaki Pref.(Obs)
Rainfall (mm)
1400
1200
1000
800
600
400
200
0
0
12
24
36
48
60
72
Forecast time (hour)

Fig. 13

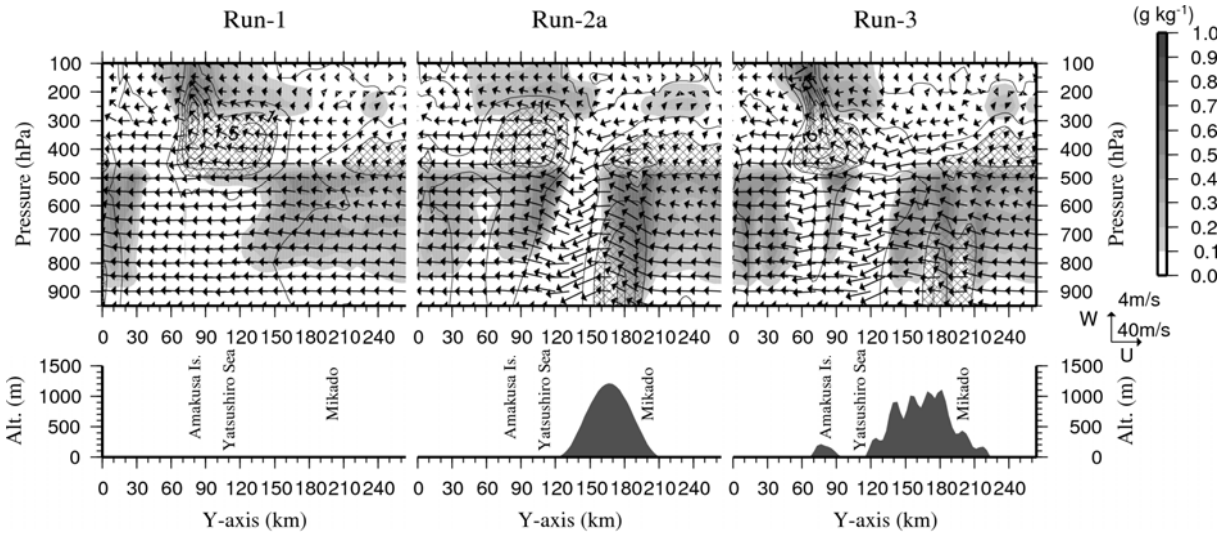
Run-1
Run-2a
Run-3
(g kg-1)
1.0
0.9
0.8
0.7
0.6
0.5
0.4
0.3
0.2
0.1
0.0
Pressure (hPa)
100
200
300
400
500
600
700
800
900
1.5
0 30 60 90 120 150 180 210 240
4m/s
W
40m/s
U
Alt. (m)
1500
1000
500
0
Amakusa Is.
Yatsushiro Sea
Mikado
Y-axis (km)